Experimental and Numerical Investigation of Vortex Flow over a Sideslipping Delta Wing

Nick G. Verhaagen* and Steven H. J. Naarding†
Delft University of Technology, Delft, the Netherlands

The influence of sideslip on the flow about a sharp-edged biconvex delta wing of a unit aspect ratio is investigated using flow visualization techniques as well as pressure and force balance measurements. The tests have been carried at a constant incidence of 21.1 deg and at angles of sideslip ranging from 0 to 20 deg. The freestream velocity was 44 m/s, corresponding to a Reynolds number of 2.5×10^6, based on root chord. Up to 12-deg sideslip, the asymmetry of the vortex crossflow and surface pressure distribution depends on the increasing symmetry in the strength and position of the vortices, as well as on boundary-layer transition. At layer angles of sideslip, the vortex flow and pressure distribution is additionally influenced by asymmetric bursting. The flow about the yawed wing is computed using a slender-body free-vortex-sheet method. Good agreement is obtained with experimental data on the part of the wing away from the apex and trailing edge.

Nomenclature

A = aspect ratio, $= b^2/S$
b = wingspan, m
C_N = normal-force coefficient, = (normal force)/$q_\infty S$
C_l = rolling-moment coefficient, = (rolling moment)/$q_\infty Sb$
C_m = pitching-moment coefficient referenced to wing apex, = (pitching moment)/$q_\infty Sc_0$
c_N = local normal-force coefficient,

$$= \frac{1}{2s}\int_{-s}^{s} \Delta c_p \, dy$$

c_p = static-pressure coefficient, $= (p - p_\infty)/q_\infty$
c_{p_t} = total-pressure coefficient, $= (p_t - p_{t\infty})/q_\infty$
c_0 = wing-root chord, m
p = static pressure, Pa
p_t = total pressure, Pa
q = dynamic pressure, Pa
Re = Reynolds number $= U_\infty c_0/\nu$
S = wing area, m^2
s = local wing semispan, m
t = local wing thickness, m
U_∞ = freestream velocity, m/s
x,y,z = wing-axes system, origin in wing apex, m
α = angle of attack, deg
β = angle of sideslip, deg
ν = kinematic viscosity, kg/ms

Subscripts
br = breakdown
g = geometric
∞ = freestream

Received Aug. 26, 1988.

*Research Associate, Faculty of Aerospace Engineering.
†Research Engineer; presently with Convex Computer, Utrecht, the Netherlands.

Introduction

THIN slender wings with highly swept and relatively sharp leading edges are employed for several modern aircraft. At moderate and high angles of attack, the flow over such wings separates at the leading edges, resulting in a steady and stable so-called leading-edge vortex flow. At zero sideslip, the leading-edge vortices are of equal strength and size, yielding a symmetric crossflow pattern and wing surface pressure distribution. Detailed experimental data on this type of symmetric vortex flow is available from many investigations carried out on slender delta-like wings or strake-wing configurations. This data is used for a better understanding of the structure of leading-edge vortices, as well as for the correlation and evaluation of theoretical flow models. Several computational methods for the simulation of the vortex flow about slender wings have been developed in recent years. Surveys of these methods are given by Hoeijmakers[1] and Newsome and Kandil.[2]

Less experimental data is available on the influence of sideslip on the flow characteristics of delta wings. Yaw effects can be important for the stability and control of aircraft at high-α flight conditions occurring during takeoff, landing, and maneuvering. Experimental investigations on yawed delta wings were carried out by Harvey[3] and Hummel,[4,5] among others, while theoretical models were developed by Pullin,[6] Jones,[7] and Luckring et al.[8] Although the quoted experimental investigations do indicate important effects of yaw on the overall aerodynamic characteristics, for the evaluation of numerical codes additional data is needed on the shape of the free shear layers, the vortex strength, the boundary-layer transition, and the surface pressure distribution, for example. Since at sideslip vortex core bursting occurs over the wing at a lower incidence than at zero sideslip, it is also essential to quantify the influence of this phenomenon.

The objective of the investigation reported in this paper, therefore, is to provide detailed experimental data on the influence of yaw on the vortex flow structure and local aerodynamic characteristics. The vortex flow was studied using a laserlight sheet facility and total pressure surveys. The boundary layer on the upper wing surface was examined using an oil-flow technique. In addition, the surface pressure distribution and the forces and moments were measured. Finally, a numerical investigation was performed using a higher-order panel method.

The paper describes the wind-tunnel tests and presents the experimental results. Subsequently, upon describing the computational method, the numerical results are compared with the experimental data. The full data report on the investigation is given in Ref. 9.

Experimental Setup

Wind-Tunnel and Test Conditions

The investigation was carried out in the low-speed wind tunnel of the Delft University of Technology, Faculty of Aerospace Engineering. The wind-tunnel test section has an octagonal cross section 1.25-m high × 1.80-m wide, and a turbulence level of about 0.05% at the freestream velocity of 44 m/s used for the present investigation. The corresponding Reynolds number, based on root chord, was 2.5×10^6.

The models were suspended at $x/c_0 = 0.80$ in the plane of symmetry through a single strut connected to a six-component balance system. The measurements were performed at a geometric $\alpha = 20.1$ deg. This angle of attack was chosen because for this incidence data at zero sideslip is available from earlier detailed flowfield surveys.[10] Angles of yaw ranged from −20 to 20 deg.

Models

Two 76-deg swept delta-wing models of identical geometry were used. The models had a root chord of 0.85 m and an aspect ratio of 1. Both models consisted of a steel core covered with wood that was sanded into shape. The steel leading and trailing edges had a thickness of 0.2 mm. Perpendicular to the root chord the cross sections were circular biconvex, while along the root chord the wing thickness satisfied the relation

$$t/c_0 = 0.056\ [x/c_0 - (x/c_0)^{5.9}]$$

The maximum thickness was 3.2% c_0. One model was sprayed black to provide sufficient contrast for flow visualization. The other model was sprayed with a transparent lacquer after being fitted with 37 thin tubes in its upper surface. Into these tubes, positioned on rays through the apex, a total of 400 0.5-mm-diam orifices were drilled. The orifices were located on 13 spanwise rows, from $x/c_0 = 0.05$ to 0.99. This model was used for the static pressure measurements only; all other tests were performed with the black model.

Flow Visualization

To study the vortex crossflow structure, a smoke/laserlight-sheet facility was used. The smoke, consisting of small paraffin oil droplets, was injected into the flow from two smoke pipes upstream of the model. The laserlight sheet was produced by a 5-W Argon-ion laser in conjunction with a cylindrical lens. The laser and optics were mounted on a bar that could be tilted and rotated such that the light sheet remained perpendicular to the model xy plane. The bar is supported by an x-traversing platform alongside the test section, enabling a translation along the tunnel axis. To obtain sufficiently dense smoke in the vortices, the freestream velocity had to be lowered to 30 m/s. The crossflow patterns were photographed by a remotely controlled camera mounted in a streamlined cover in the diffuser of the wind tunnel. Photographs of the crossflow patterns from $x/c_0 = 0.40$ to 1.20 were taken at angles of sideslip ranging from 0 to 20 deg.

The flow on the upper surface of the model was visualized using oil consisting of titanium dioxide and kaolinum powder (china clay) mixed with kerosene and pure oleic acid fluid. The surface-streamline patterns were photographed at slip angles ranging from 0 to 20 deg.

Pressure and Balance Measurements

The surface pressure distribution was determined by consecutively measuring the pressure distribution at each of the 13 spanwise rows of orifices. Since in each of the 37 pressure tubes the orifices were mutually connected by the tube itself, the spanwise pressure distribution at one specific row could only be measured by sealing off the pressure holes at the 12 other rows. This was done by using strips of 0.04-mm-thin adhesive tape. The spanwise pressure distributions were measured at slip angles from −20 to 20 deg. The pressure tubes of the model were connected to a multimanometer that automatically records the spanwise pressure distribution.

The leading-edge vortex center was located by tracing the total pressure minimum with a Kiel probe. This total pressure probe was mounted on a computer-controlled traversing mechanism positioned in the diffuser of the wind tunnel. This mechanism, used before for the entrainment investigation described in Ref. 10, enables the probe to be traversed in planes perpendicular to the tunnel axis. To reduce the angle between the probe and the vortex axis, the probe-carrying sting of the traversing mechanism was bent such that the probe axis made an angle of approximately 5 deg with the suction side of the wing. Probe sensitivity tests showed that the Kiel tube was insensitive to flow direction for angles up to 20 deg. To avoid larger angles, the probe was fixed at a sideslip angle of 20 deg for the traverses through the windward vortex and at −20 deg for those through the leeward one. Traverses were made at $x/c_0 = 0.10, 0.20, 0.40, 0.60, 0.80$, and 1.00 for positive angles of sideslip only.

Balance measurements were performed using a six-component balance system. Corrections were applied for aerodynamic interference between strut and model and for deflection of the strut under aerodynamic load. The angle of attack and the aerodynamic coefficients were, in addition, corrected for blockage and lift effects following methods suggested by Garner and Rogers[11] for the case of zero sideslip. Although these methods were developed for attached-flow conditions, Karou[12] has shown that, at zero sideslip, they can be applied successfully for flows with leading-edge vortices. The corrected angle of attack has a value of 21.1 deg. Since, to the authors' knowledge, no proven correction method is available to calculate the effect of wall constraint for yawed delta wings, no further corrections were applied. Data acquisition, storage, and processing of the pressure and balance measurements were computer controlled.

Experimental Test Results

Vortex Flow Visualization

In Fig. 1, pictures of the laserlight-sheet flow investigation are shown, taken at $x/c_0 = 0.60$, 1.00, and 1.20. The laser is located on the port side of the wing. To avoid confusion, it should be remarked that in the pictures of $x/c_0 = 0.60$, a mirror image of the leading-edge vortices is visible on the black shining wing surface. Furthermore, note that at $\beta = 20$ deg the attacking edge is not lit due to the curvature of the model illuminated from the port side.

In the photographs the subcore shows up as a dark circular spot in the center of the vortex. This is a consequence of the lack of light-scattering particles in this region, a phenomenon commonly observed in laserlight-sheet visualization and laser Doppler velocimetry experiments. This "black hole" is caused by the high circumferential velocities at the edge of the subcore, through which the relatively heavy smoke particles approaching this region are driven out. In addition, the high axial velocities in the subcore tend to reduce the density of the smoke. The pictures on the left-hand side of Fig. 1 show the well-known symmetrical vortex crossflow pattern for zero sideslip. Near the leading edge a secondary vortex is visible. Downstream of the trailing edge, double-branched "trailing-edge" vortices are formed that have a sense of rotation opposite to that of the corresponding leading-edge vortex. Although the trailing-edge vortices have the same sense of rotation as the secondary ones, these are separate vortices originating at the trailing edge.[13] This is confirmed by numerical simulation[1] where the trailing-edge vortices result from inviscid wake rollup.

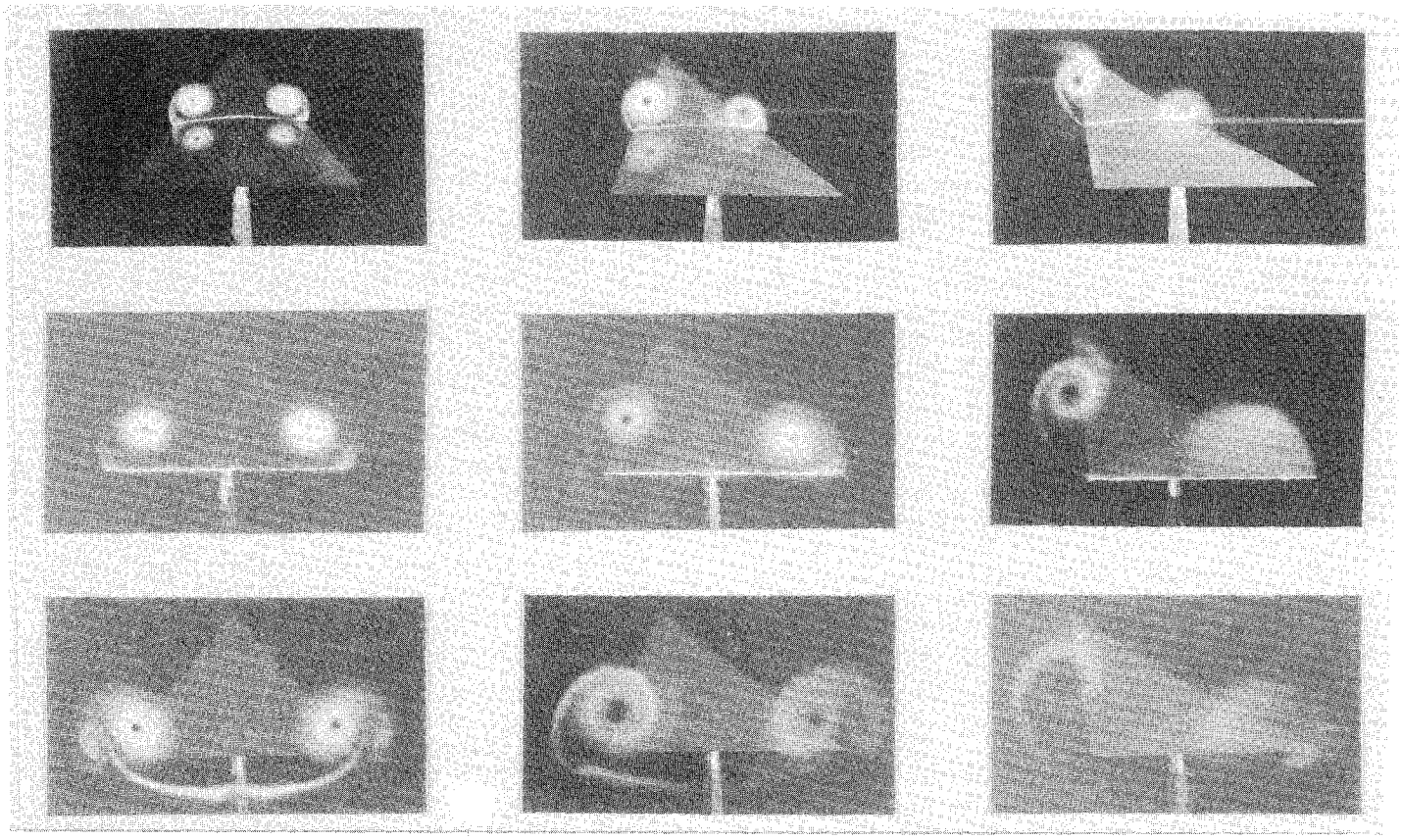

Fig. 1 Effect of angle of sideslip on the vortex flow for various chordwise locations, $\alpha = 21$ deg.

The effect of sideslip is evident from the other pictures of Fig. 1. With increasing sideslip the windward leading-edge vortex moves inward and closer to the surface of the model, while the leeward vortex moves outward and away from the model. The core of the latter vortex moves outboard of the leading edge at yaw angles beyond 16 deg, for which the retreating leading edge becomes a trailing edge. As a result of these displacements, the windward shear layer tightens and adopts a more elliptical shape, while the leeward shear layer becomes longer and more circular.

The secondary vortex on the attacking wing half remains visible at all angles of sideslip. This is not the case on the retreating wing half, where the secondary vortex disappeared from the smoke picture already at a small angle of sideslip. On this half of the wing, smoke could only be fed into the free shear layer by impinging it on the lower surface. As a consequence, most smoke was concentrated in the primary vortex, leaving no smoke to visualize the secondary vortex at the same time. However, as will be shown later, the oil-flow investigation gives clear evidence of the presence of a secondary separation on the retreating half of the wing.

At the trailing edge, both leading-edge vortex subcores remain visible up to $\beta = 12$ deg. Beyond this value of the angle of sideslip, the subcore on the attacking wing half starts to disappear, indicating that bursting has reached the trailing edge. This value agrees with results of Hummel.[4] Vortex bursting is a rather complex and unsteady phenomenon, making it difficult to determine its onset. The burst was observed to move rapidly back and forth along the vortex axis over a distance of about 10% c_0. Its upstream movement with sideslip and the range of possible locations are given in Fig. 2. Included in this figure are the breakdown locations found using a tuft probe. The breakdown point is very sensitive to yaw in the vicinity of the trailing edge; from 12- to 13-deg sideslip the burst moves more rapidly upstream than at the higher angles. Similar sensitivity to the angle of attack of the burst point has been observed by McKernan and Nelson.[14] It is associated with a high gradient in the pressure distribution along the vortex axis in the vicinity of the trailing edge. The breakdown location found on the rear quarter of the wing using the tuft tube is 5% c_0 more upstream than that found from the laserlight-sheet investigation. More forward on the wing, the difference between both techniques in less. This is similar to the results of seven-hole probe/vortex breakdown point interference observations,[4,15] where it was found that near the trailing edge breakdown is more sensitive to the insertion of a probe than at a more forward location.

The pictures at the bottom of Fig. 1 show the evolution of the flow downstream of the model. With increasing sideslip, the windward trailing-edge vortex swirls faster around its accompanying leading-edge vortex. The leeward trailing-edge vortex becomes weaker with increasing sideslip and has disappeared completely at about 12-deg sideslip. At this angle, the bound vorticity on the leeward half of the trailing edge has apparently reduced to such an extent that no concentrated trailing-edge vortex is formed. From 4- to 20-deg sideslip, ripples were locally visible in the leeward shear layer at $x/c_0 = 1.20$, but at some sideslip angles also near the trailing edge. It is not known whether these ripples are caused by disturbances from the smoke pipes upstream of the model or by inherent instability of the shear layer.

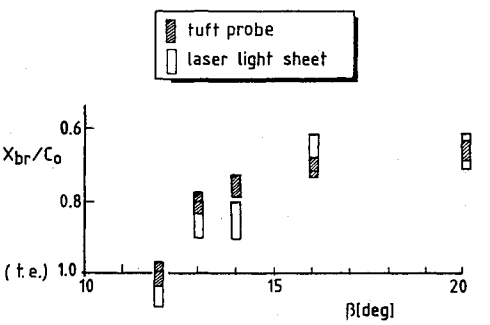

Fig. 2 Windward vortex core burst position vs angle of sideslip, $\alpha = 21$ deg.

Total Pressure Measurements

Figure 3 gives the evolution with sideslip of the total pressure coefficient in the vortex core at $x/c_0 = 0.60$ and at the trailing edge. It shows that the total pressure coefficient of the leeward vortex increases with sideslip. This indicates that the strength of this core reduces with increasing sideslip, or with increasing effective angle of leading-edge sweep. The opposite is found for the windward vortex. Total head measurements by Harvey[3] suggest that the strength of the secondary vortex cores varies like their associated primary vortex core. The total pressure coefficient of the windward primary vortex decreases to $\beta = 12$ deg when vortex breakdown has reached the trailing edge. Beyond this angle, at $x/c_0 = 0.60$ the decrease of the total pressure coefficient, or the increase of the vortex strength, stagnates. Since the vortex breakdown point will not reach this chordwise station at sideslip angles below 20 deg, this indicates that breakdown also affects the vortex flow upstream of the breakdown point. Further evidence of this will be obtained from the static pressure measurements. Near the the trailing edge, no clear total pressure minimum could be found beyond 12-deg sideslip. Downstream of the burst point a wide region of low total pressure was measured, indicating that there was still some vorticity retained in the core. However, the radial total pressure gradient had reduced significantly, and no clear-cut minimum could be distinguished. Rapid pressure fluctuations gave evidence of a high level of turbulence in the broken-down core. Similar results have been measured by Payne et al.[15]

Surface Flow and Static Pressure Distribution

Figure 4 shows the schematic upper-surface streamline pattern for different angles of sideslip. Also shown in this figure are the projection of the vortex axes, as determined from the total pressure surveys, and the mean location of the bursting point. The influence of sideslip on the surface pressure distribution is demonstrated in Figs. 5–7, where the spanwise distributions are shown for $x/c_0 = 0.30$, 0.60, and 0.90, respectively.

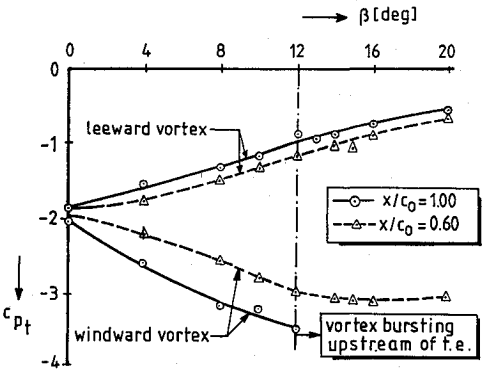

Fig. 3 Effect of angle of sideslip on total pressure coefficient at $x/c_0 = 0.60$ and 1.00, $\alpha = 21$ deg.

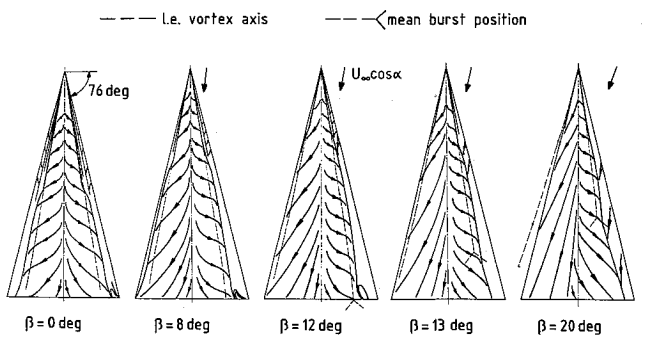

Fig. 4 Vortex axis position and upper-surface streamline pattern at various angles of sideslip, $\alpha = 21$.

In the upper-surface streamline pattern for $\beta = 0$ deg (Fig. 4a), boundary-layer transition is evident from a kink in the secondary separation line at $x/c_0 = 0.52$. Upstream of this station, the laminar separation line is located at a spanwise location $y/s = 0.65$, while downstream of it the now turbulent boundary layer separates more outward at $y/s = 0.83$. In the case of the laminar boundary layer, the suction induced by the primary and secondary vortices is more or less equal in magnitude, as is evident from Fig. 5a. When the boundary layer has become turbulent, the separation closer to the leading edge results in a weaker secondary vortex than in the case of a laminar boundary layer. Consequently, the primary vortex draws closer to the wing and shifts slightly toward the leading edge.[4,16] This results in a higher suction peak underneath the primary vortex and in less suction underneath the secondary vortex (Fig. 6a).

When the wing is yawed to 20 deg, the spanwise suction induced on the forward part of the windward wing half increases continuously because primary and secondary vortices increase in strength and draw closer to the wing upper surface (Fig. 5). On the rear part of this wing half, this is true up to $\beta = 12$ deg (Fig. 6a). At larger angles of sideslip the suction peak downstream of $x/c_0 = 0.50$ reduces due to the upstream influence of vortex bursting (Fig. 6b). Since the windward primary vortex also moves slowly toward the centerline, the suction peak shifts slightly inward as well. The described effects result in a slight shift of the secondary separation line toward the wing centerline (Fig. 4). On the rear part of the wing, the windward primary and secondary vortices bend into the freestream direction. Consistent with this, the secondary separation line curves toward the wing centerline.

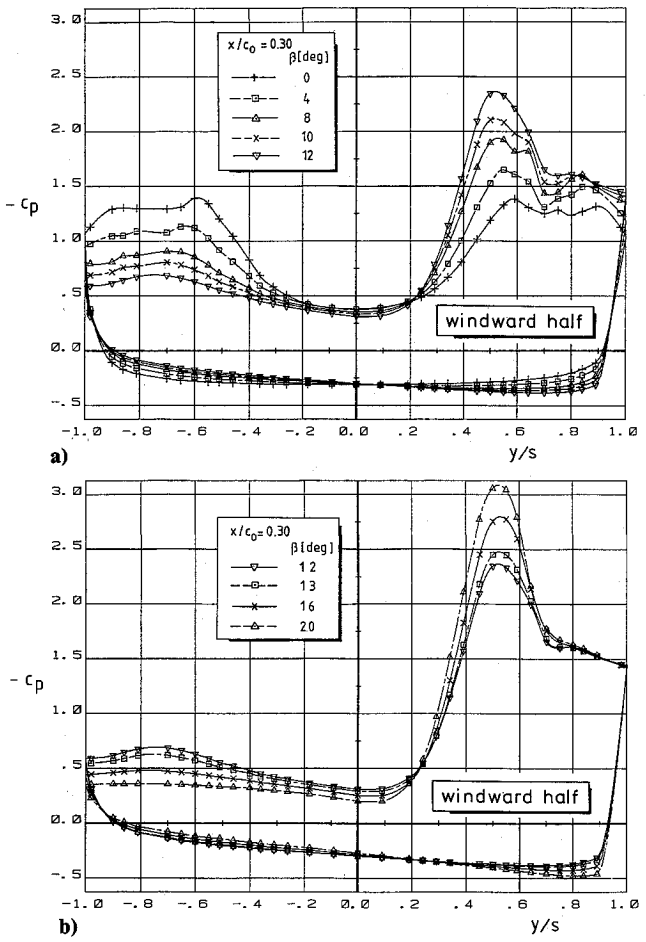

Fig. 5 Effect of angle of sideslip on the spanwise pressure distribution at $x/c_0 = 0.30$, $\alpha = 21$ deg; a) 0–12-deg sideslip; b) 12–20-deg sideslip.

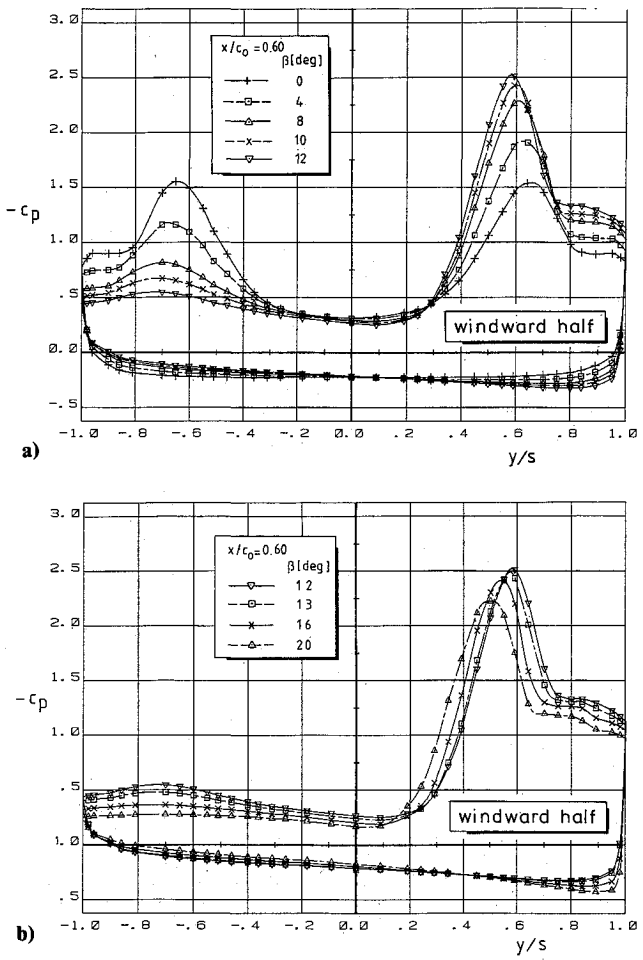

Fig. 6 Effect of angle of sideslip on the spanwise pressure distribution at $x/c_0 = 0.60$, $\alpha = 21$ deg; a) 0–12-deg sideslip b) 12–20-deg sideslip.

On the leeward wing half of the yaw effects are opposite to those on the windward half; the suction peak decreases in height and shifts outward with increasing yaw. Due to the decreasing spanwise pressure gradient, the leeward secondary separation line shifts toward the retreating leading edge. Beyond $\beta = 12$ deg, downstream of the transition region this line could hardly be distinguished, indicating that the turbulent boundary layer remains attached up to the leading edge. At $\beta = 20$ deg, the pressure distribution on the retreating wing half is almost flat. It is, therefore, not surprising that at this slip angle it was impossible to distinguish even the laminar part of the secondary separation line. On the lower wing surface the positive pressure on the windward half of the wing increases with yaw, while that on the leeward half decreases. As has also been found by Harvey,[3] the point of highest positive pressure moves toward the attacking leading edge, indicating that the stagnation point moves toward this edge with increasing sideslip.

The displacement of the boundary-layer transitional region with sideslip is visible in Fig. 4. On the left and right wing halves the transitional region can be seen to move upstream with increasing sideslip. These results hold for the flow-visualization model, hence without pressure orifices and sealing tape. Taping causes an upstream shift of the transitional region. For example, the surface pressure distribution for $\beta = 10$ deg suggests boundary-layer transition between $x/c_0 = 0.20$ and 0.30, while the oil-flow pattern indicates transition at approximately $x/c_0 = 0.40$.

Up to $\beta = 12$ deg, the suction peak on the windward wing half increases with sideslip at all chordwise stations. At larger slip angles the same tendency is found on the forward part of the wing (Fig. 5b). However, downstream of $x/c_0 = 0.50$, the

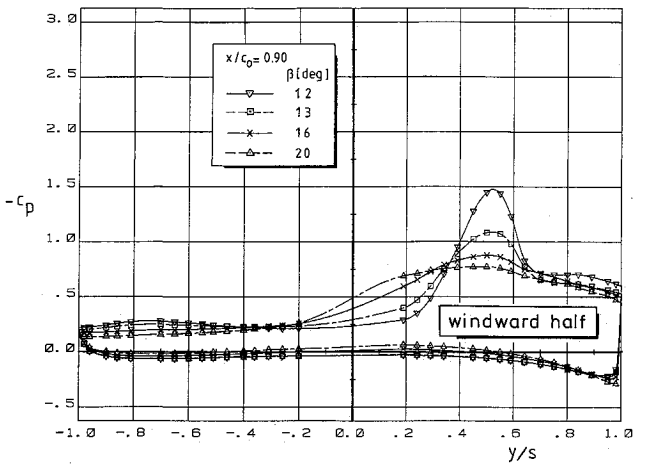

Fig. 7 Spanwise pressure distribution at $x/c_0 = 0.90$ from 12 to 20 deg sideslip, $\alpha = 21$ deg.

suction no longer increases and even reduces with increasing sideslip (Fig. 6b). Such an increase in pressure upstream of the burst has similarly been observed in other experiments.[14,18] It is probably due to the stagnation of the flow upstream of the burst. The largest reduction of suction occurs downstream of the burst. The latter is illustrated in Fig. 7, where the pressure distribution at $x/c_0 = 0.90$ is given for $\beta = 12$ and beyond. At $\beta = 12$ deg, the vortex core bursts downstream of $x/c_0 = 0.90$, while at $\beta = 13$ deg and beyond, bursting occurs upstream of this station (Fig. 2). During the measurements fluctuations were observed in the surface pressures on the windward wing half as soon as the vortex burst approached the measuring station. These fluctuations indicate the unsteady nature of the breakdown phenomenon. Downstream of the burst point the suction of the primary and secondary vortices reduces, while the suction on the central part of the wing increases. Bursting causes a radial expansion of the vortex core, through which circulation previously contained in a narrow core is redistributed over a wider area. Since the spanwise pressure gradient reduces as well, secondary separation is delayed to a position closer to the leading edge. In the surface streamline pattern, bursting is clearly marked by a second outward bending of the secondary separation line (Fig. 4). The bend is at a short distance downstream of the burst point. Because of the unsteadiness of the burst point, no attempt has been made here to estimate this distance.

Balance Measurements

In Fig. 8, the variation with sideslip of the normal force coefficient C_N, the pitching moment coefficient C_m, and the rolling moment coefficient C_l is shown. These forces and moments are given with respect to the model system of axes, with the apex as the origin.

Up to $\beta = 12$ deg, C_N reduces slightly with increasing sideslip due to a slight reduction of the loading on the rear part of the wing. Because of this effect, C_m gradually increases with yaw. The increasing asymmetry of the spanwise pressure distribution results in an increasing negative value of C_l with sideslip.

To determine accurately the angle where bursting occurs, in the force balance measurements $\beta = 12.5$ deg was included. The sharp change in the force and moment curves confirms that breakdown occurs over the wing from $\beta = 12$ deg onward. As a result of the rapid upstream travel of the burst point and the associated abrupt reduction of the suction peak downstream of it, C_N and C_m decrease considerably between 12 and 12.5 deg. When the slip angle is further increased to 20 deg, these coefficients reduce more gradually. As far as C_l is concerned, bursting initially counteracts the tendency to roll, but with increasing sideslip this moment increases again, albeit at a lower rate. The latter is due to the fact that suction is now induced on a smaller part of the windward wing half.

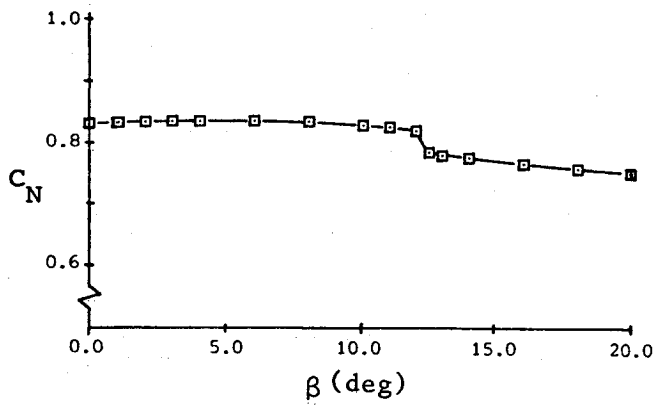

a) Normal force

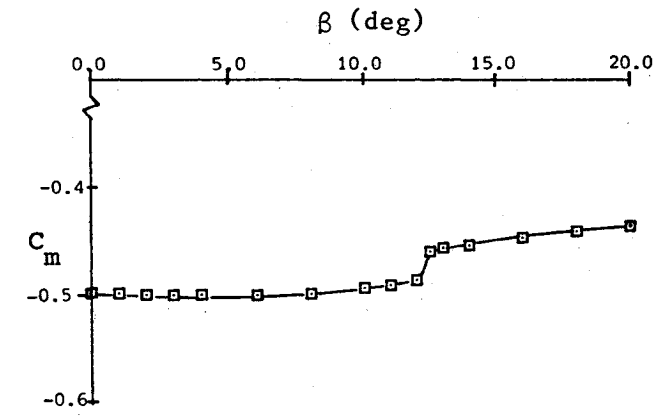

b) Pitching moment

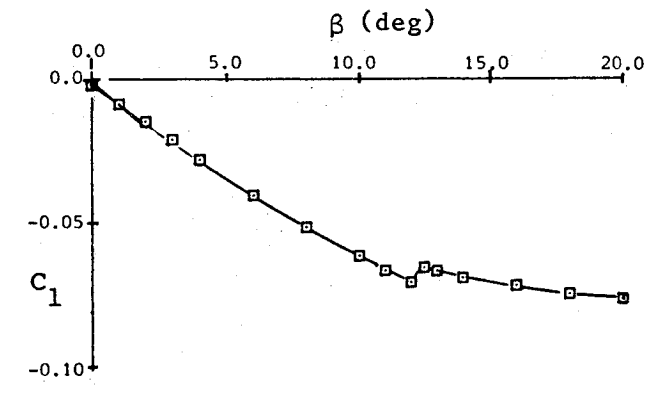

c) Rolling moment

Fig. 8 Effect of angle of sideslip on wing force and moment characteristics, $\alpha = 21$ deg.

Computational Results

The flow about the yawed delta wing has been calculated using the VORSBA computational method (Vortex Slender Body Approximation). This free vortex sheet (FVS) code has been developed by Hoeijmakers and is described in detail in Ref. 19. In the potential flow model the variations in streamwise direction are assumed to be small compared to those in the crossflow plane. The three-dimensional problem is thus reduced to a sequence of relatively simple two-dimensional crossflow plane problems where the boundary conditions account for the three-dimensionality of the problem. The crossflow plane geometry may consist of any number of segments, either portions of the solid geometry or vortex sheets. For the present biconvex delta wing the crossflow plane geometry is composed of four mutually connected segments. The wing is modeled by two segments. The upper wing surface segment carries a source distribution needed to model wing thickness, while for the lower wing surface a doublet distribution is used. The spiraling free shear layers are represented by vortex sheet segments carrying a doublet distribution. The sheet segments, which are abutted to the leading edges, end in a line vortex/feeding sheet combination. The position of the vortex sheet and core and the singularity distributions are calculated by VORSBA as part of the solution. Subsequently, the surface pressure distribution is computed. In the present study, a total of 80 panels were used, 20 panels on each segment. Secondary separation and entrainment effects have not been included in the present numerical model.

The effect of sideslip was considered at $x/c_0 = 0.60$, because at this station 1) much experimental data is available, 2) the boundary layer is turbulent, which reduces the influence of the secondary vortex, 3) the apex and the trailing-edge effects are small, and 4) no bursting occurs. The crossflow has been computed using a "single-step" conical flow approximation. In that case, the geometry and the flow are assumed to be conical from the apex to the station considered. This is a reasonable approximation since the geometry of the forward half of the wing is nearly conical as well. Up to 12-deg sideslip, the vortex sheet length was held fixed at a value of twice the local semispan(s). The flow visualization tests show that with sideslip the leeward vortex sheet moves away from the surface and becomes less tightly wound, while the windward vortex sheet becomes more tightly rolled up. To enable the leeward sheet to complete a full revolution, it was decided to lengthen this sheet to 2.1 s for slip angles beyond 12 deg. For the same reason, the more tightly wound windward sheet was cut to a length of 1.9 s. In Fig. 9, the results are shown for $\beta = 0$, 10, and 20 deg. The calculated vortex sheets shown in the leftside figures compare very well qualitatively with the laserlight-sheet visualization results. As far as the position of the vortex axes is concerned, increasing differences can be noted with sideslip. The vertical position of the windward vortex is well predicted, but its lateral position is overestimated. The same tendency was found by Pullin,[6] who calculated the vortex flow over a yawed flat-plate delta wing up to 15-deg incidence using a modified Mangler and Smith slender-body theory FVS model. This discrepancy is attributed to the neglect of the secondary vortex, whose increasing size and strength forces the primary vortex inward. Since the influence of the secondary vortex on the leeward wing half decreases with increasing sideslip, it was expected that the position of the leeward vortex axis would be better predicted. This appears to be true for the lateral position, but the computed vertical position exceeds the measured one more and more with increasing sideslip. This will need further investigation.

The spanwise pressure distribution depicted in Fig. 9 evolves in the same fashion with sideslip as the experimental distribution. The pressure distributions computed for $\beta = 0$ and 10 deg compare reasonably well with the measurements. As a matter of fact, this holds for all computed pressure distributions up to 12-deg sideslip. The largest discrepancies are due, again, to the neglect of the secondary vortices. Beyond $\beta = 12$ deg, vortex breakdown effects on the attacking wing half have a large influence. These effects are not included in the present solution and result in an overestimation of the suction peak.

The conical approximation does not apply to the rear part of the wing where the influence of the trailing edge is felt. As a result, there are considerable differences between the computed and measured wing forces and moments.[9] Nevertheless, the agreement between the numerical and experimental results on the central part of the wing is very promising and stimulates further development of the present code.

Conclusions

The influence of sideslip on the flow of a 76-deg swept sharp-edged biconvex delta wing was investigated at a constant angle of attack of 21.1 deg and angles of sideslip ranging from 0 to 20 deg. Laserlight-sheet and oil-flow visualization tests

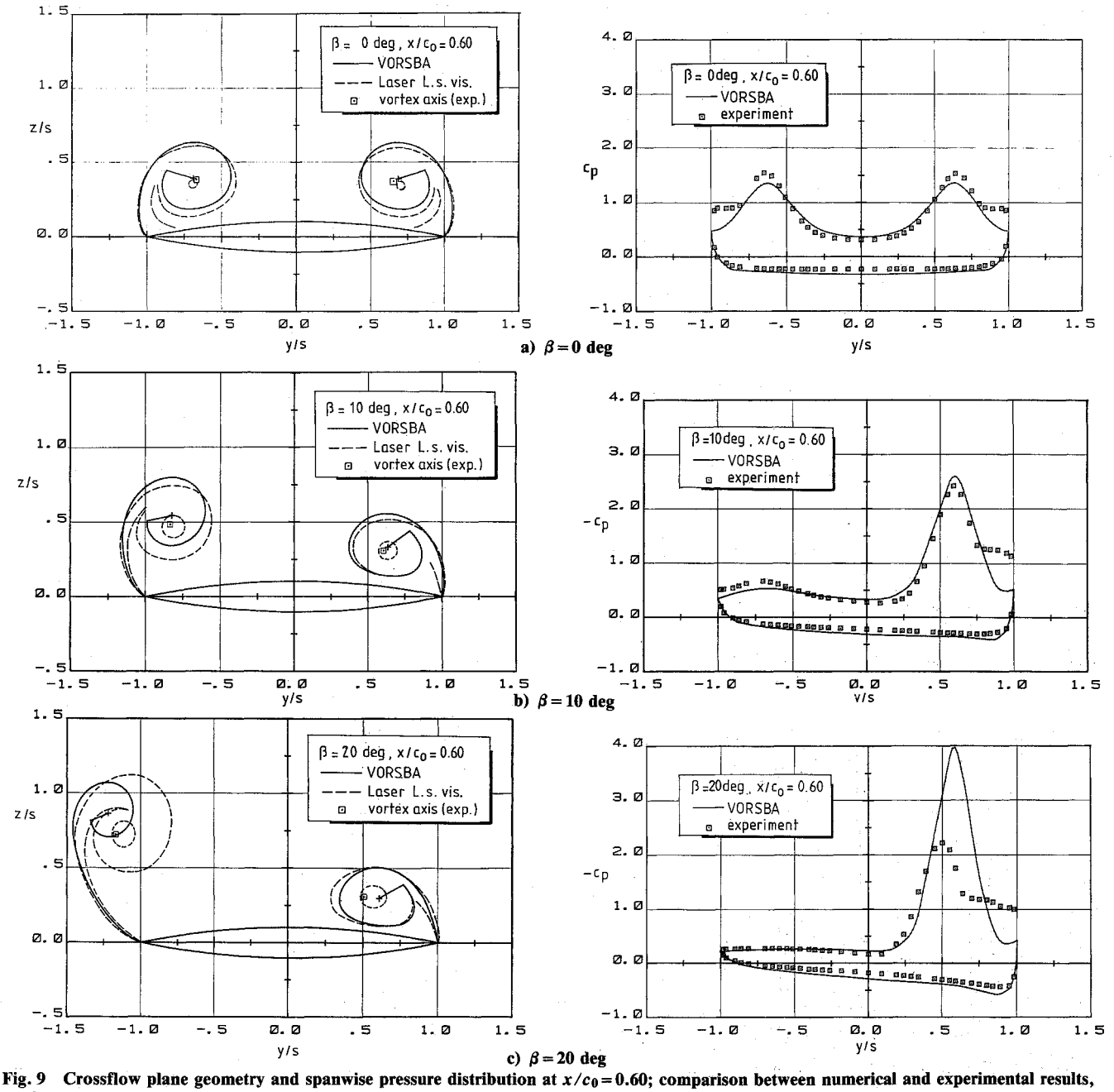

Fig. 9 Crossflow plane geometry and spanwise pressure distribution at $x/c_0 = 0.60$; comparison between numerical and experimental results, $\alpha = 21$ deg.

were used to reveal the evolution of the vortex crossflow structure as well as the surface streamline pattern. Total pressure surveys were carried out to measure vortex axis positions as well as the total pressure distribution along the vortex axis. Detailed surface pressure measurements were made to explain the measured forces and moments.

Up to $\beta = 12$ deg, the asymmetric crossflow structure and surface pressure distribution alter gradually with sideslip due to changes in vortex strength and position and to boundary-layer transition. At larger angles of sideslip, vortex breakdown on the rear part of the wing has an additional influence on the vortex structure and surface pressure distribution, both downstream and to a lesser extent upstream of the burst point. Behind the trailing edge no trailing-edge vortex is formed.

The VORSBA computer code satisfactorily predicts the general changes due to sideslip of the vortex crossflow structure and static pressure on the central part of the wing. Discrepancies are due to the neglect of the secondary vortex and the inability to calculate the effect of vortex breakdown. Further development of the code is needed to include at least secondary separation and trailing-edge effects. For the validation of numerical codes, additional experiments are required to obtain data at other angles of attack and Reynolds numbers.

Acknowledgments

The authors are indebted to the Dutch National Aerospace Laboratory (NLR) and in particular to H. W. M. Hoeijmakers, for the use of the VORSBA computer code. The authors also wish to expres gratitude to J. E. Lamar of NASA Langley Research Center, Hampton, VA, for valuable discussions. The authors would also like to thank P.N.J. Deken and F. A. Bazen for the installation and operation of the laserlight-sheet equipment.

References

[1]Hoeijmakers, H. W. M., "Methods for Numerical Simulation of Vortical Flow," *Studies of Vortex Dominated Flows*, edited by M. Y. Hussaini and M. D. Salas, Springer-Verlag, 1987, pp. 221-269.

[2]Newsome, R. W. and Kandil, O. A., "Vortical Flow Aerodynamics—Physical Aspects and Numerical Simulation," AIAA Paper 87-0205, Jan. 1987.

[3]Harvey, J. K., "Some Measurements on a Yawed Slender Delta

Wing with Leading-Edge Separation," Aeronautical Research Council, ARC R&M 3160, Oct. 1958.

[4]Hummel, D., "Untersuchungen über das Aufplatzen der Wirbel an schlanken Deltaflügeln," *Zeitschrift der Flugwissenschaft,* Vol. 13, No. 5, 1965, pp. 158–168.

[5]Hummel, D., "Experimentelle Untersuchung der Strömung auf der Saugseite eines Schlanken Deltaflügels," *Zeitschrift der Flugwissenschaft,* Vol. 13, No. 7, 1965, pp. 247–252.

[6]Pullin, D. I., "Calculations of the Steady Conical Flow Past a Yawed Slender Delta Wing with Leading-Edge Separation," Aeronautical Research Council R&M 3767, July 1972.

[7]Jones, I. P., "Flow Separation from Yawed Delta Wings," *Computers & Fluids,* Vol. 3, 1975, p. 155–177.

[8]Luckring, J. M., Schoonover, J. R., and Frink, N. T., "Recent Advances in Applying Free Vortex Sheet Theory for the Estimation of Vortex Flow Aerodynamics," AIAA Paper 82-0095, Jan. 1982.

[9]Naarding, S. H. J. and Verhaagen, N. G., "Experimental and Numerical Investigation of the Vortex Flow over a Sharp-edged Delta Wing; With and Without Yaw," Delft University of Technology Rept. LR-573, Dec. 1988.

[10]Verhaagen, N. G. and Kruisbrink, A. C. H., "The Entrainment Effect of a Leading-Edge Vortex," *AIAA Journal,* Vol. 25, Aug. 1987, pp. 1025–1032.

[11]Garner, H. C. and Rogers, E. W. E., "Subsonic Wind-tunnel Wall Corrections," AGARDograph 109, 1966.

[12]Karou, A., "Separated Vortex Flow over Slender Wings between Side Walls; Theoretical and Experimental Investigation," Delft University of Technology, Rept. LR-300, Aug. 1980.

[13]Hummel, D., "On the Vortex Formation over a Slender Wing at Large Angles of Incidence," AGARD CP 247, Paper 15, 1978.

[14]McKernan, J. F. and Nelson, R. C., "An Investigation of the Breakdown of the Leading Edge Vortices on a Delta Wing at High Angles of Attack," AIAA Paper 83-2114, Aug. 1983.

[15]Payne, F. M., Ng, T. T., and Nelson, R. C., "Experimental Study of the Velocity Field on a Delta Wing," AIAA Paper 87-1231, June 1987.

[16]Kjelgaard, S. O., Sellers, W. L., III, and Weston, R. P., "The Flowfield over a 75-Degree Swept Delta Wing at 20.5 Degrees Angle of Attack," AIAA Paper 86-1775, June 1986.

[17]Carcaillet, R., Manie, F., Pagan, D., and Solignac, J. L., "Leading Edge Vortex Flow over a 75-Degree-Swept Wing—Experimental and Computational Results," International Council of the Aeronautical Sciences, Paper 86-1.5.1, 1986.

[18]Lambourne, N. C. and Bryer, D. W., "The Bursting of Leading Edge Vortices—Some Observations and Discussion of the Phenomenon," Aeronautical Research Council R&M 3282, April 1961.

[19]Hoeijmakers, H. W. M., "An Approximate Method for Computing the Flow about Slender Configurations with Vortex Flow Separation," National Aerospace Laboratory, NLR TR 8601 U, Jan. 1986.